Article

Molecular Dynamics-Based Design and Biophysical Evaluation of Thermostable Single-Chain Fv Antibody Mutants Derived from Pharmaceutical Antibodies

Kyo Okazaki,[†] Yoshihiro Kobashigawa,[†] Hikari Morita, Soichiro Yamauchi, Natsuki Fukuda, Chenjiang Liu, Yuya Toyota, Takashi Sato, and Hiroshi Morioka*

Read Online

ACCESS | Metrics & More | Article Recommendations | Supporting Information

ABSTRACT: Antibody drugs are denatured under physical stress, e.g., friction, heat, and freezing, which triggers formation of aggregates and resultant allergic reactions. Design of a stable antibody is thus critical for the development of antibody drugs. Here, we obtained a thermostable single-chain Fv (scFv) antibody clone by rigidifying the flexible region. We first conducted a short molecular dynamics (MD) simulation (3 runs of 50 ns) to search for weak spots in the scFv antibody, i.e., flexible regions located outside the CDR (complementarity determining region) and the interface between the heavy-chain and light-chain variable regions. We then designed a thermostable mutant and evaluated it by means of a short MD simulation (3 runs of 50 ns) based on reductions in the root-mean-square fluctuation (RMSF) values and formation of new hydrophilic interactions around the weak spot. Finally, we designed the VL-R66G

mutant by applying our strategy to scFv derived from trastuzumab. Trastuzumab scFv variants were prepared by using an *Escherichia coli* expression system, and the melting temperature—measured as a thermostability index—was 5 °C higher than that of the wild-type trastuzumab scFv, while the antigen-binding affinity was unchanged. Our strategy required few computational resources, and would be applicable to antibody drug discovery.
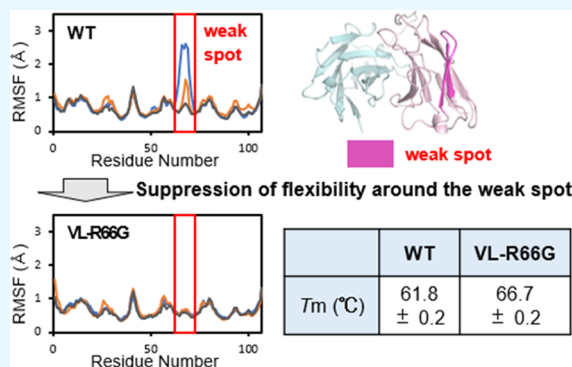
INTRODUCTION

Antibody drugs are widely used in clinical applications, and a number of new antibody drugs are under development.[1] However, antibody drugs are expensive due to the use of mammalian cells in their production. Moreover, the depletion of target molecules has shifted the development of antibody drugs to the next-generation antibodies, involving bispecific antibodies and antibody−drug conjugates, which require more sophisticated technologies. Single-chain Fv (scFv) antibodies, which consist of a heavy-chain variable region (VH) and a light-chain variable region (VL) connected by a short flexible polypeptide linker, are regarded as an attractive approach for overcoming these problems since they can be produced by using *Escherichia coli* (*E. coli*) and easily engineered by genetic techniques.[2−8] However, scFv antibodies are less stable than Fab and IgG antibodies, are more easily denatured and aggregated under physical stress, e.g., concentration, friction, heat, and freezing, and induce immune and allergic reactions that cause antidrug antibody production for decreased drug efficacies. Since denaturation triggers the formation of aggregates, the production of thermostable antibodies is critical for wide application of scFv proteins. Recently, we developed cyclic scFv, in which the N-terminus and C-terminus were connected by a peptide bond, and succeeded in

suppressing aggregation mediated by interchain VH−VL interactions.[9,10] Cyclic scFv, however, did not contribute to the improvement of thermal stability, and the suppression of aggregation through unfolding reactions remains to be overcome.

Several methods have been used to obtain thermostable scFv clones, including rational design based on the crystallographic data,[11−14] grafting of complementarity-determining regions (CDRs) to a stable framework,[15] and molecular evolution-engineering methods.[16−22] In all of these methods, it is necessary to prepare a number of scFv clones for the evaluations of the thermal stability and antigen-binding affinity, which are time- and labor-intensive tasks. Recently, the MD-based design of the thermostable variants of VHH, a single-domain antibody, was attempted.[23,24] In these studies, 5 runs of 1.1 μs (5.5 μs in total) MD simulations or 10 runs of 100 ns
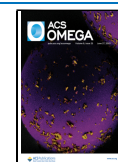
MD simulations for two or three temperature settings (2 or 3 μs in total) were performed for each mutant clone. Here, we attempted to design thermostable scFv mutants using the shorter and the smaller number of molecular dynamics (MD) simulations with markedly reduced computational resources. Our strategy began with the search for highly flexible regions of scFv proteins based on the less number (three) of the independent short (50 ns) MD simulations (150 ns in total). Highly flexible residues have a low number of contacts with other amino acids and exhibit large thermal fluctuation, which can trigger protein unfolding, making these residues a potential weak spot. Hence, mutations were introduced to rigidify such weak spots. The effects of mutation were assessed both by the changes in RMSF values and by the formation of new hydrophilic interactions (hydrogen bond or salt bridge) around the weak spot as compared to the wild-type protein. Finally, the thus-designed mutant was prepared by using an E. coli expression system, and the thermostability and antigen-binding affinity were evaluated by several biophysical techniques. The present strategy was applied to the scFv protein derived from trastuzumab (denoted as Tras-scFv); Tras-scFv, which is also known as Herceptin, recognizes HER2 and is used for the clinical treatment of breast cancer. Our results showed that the thus-obtained mutant had a melting temperature of about 5 °C higher than that of the wild-type Tras-scFv. The present strategy was also successfully applied for scFv derived from muromonab-CD3 (OKT3). The combination of a small number of independent, short MD-based identifications of flexible regions, region rigidification, and an MD-based evaluation cycle was proven to be a fast and computationally effective method for obtaining a thermostable scFv clone.

MATERIALS AND METHODS

MD Simulations. The structure of the trastuzumab Fv region was obtained from the Protein Data Bank (PDB ID: 1n8z),[25,26] and the peptide linker was modeled using the MODELLER algorithm[27−29] embedded in the UCSF Chimera software package[30] under the default modeling parameters. The scFv structure with the lowest energy was chosen from the five results, excluding the results where the linker passes through the Fv region. UCSF Chimera was used to generate the mutants. MD simulations were performed using Gromacs 2018[31] with the CHARMM36 force field and CMAP correction.[32] scFv was centered into a dodecahedron box at least 1 nm away from the box edge. The box was filled with the TIP3P water model as a solvent, and then Cl ions were added to neutralize the protein charge. Subsequently, the systems were energy-minimized using the steepest descent minimization with a tolerance of 1000 kJ/mol nm. After energy minimization, the systems were equilibrated at the constant volume (NVT) for 100 ps and the constant pressure (NPT) for 100 ps at 300 K, respectively (Figure S1). Finally, MD simulation for 50 ns at 300 K was performed 3 times, and the results were saved every 10 ps. A cutoff distance of 12 Å was applied for Coulombic and van der Waals interactions. Long-range electrostatic interactions were calculated by using the smooth particle mesh Ewald (SPME) method[33] with Verlet cutoff. The LINCS algorithm was employed to constrain bonds involving hydrogen atoms due to its calculation speed in Gromacs as compared to other bond constraint methods.[34,35] A lincs-order of 4 and a lincs-iter of a single step were used for all MD simulations. PyMOL, UCSF Chimera, and VMD[36]

software were used for analyzing and visualizing the MD trajectories. The root-mean-square fluctuation (RMSF) data were exported on the basis of trajectories beginning from 20 ns to allow for relaxation at the beginning of the simulation.

Construction of Plasmids. The coding sequences for Tras-scFv and for scFv derived from muromonab-CD3 (OKT3) (denoted as OKT3-scFv) were cloned into pET-28b(+) plasmids. A hexahistidine tag was attached to the C-terminus to allow for purification by affinity chromatography using Ni-NTA agarose resin (WAKO).[37] The resultant plasmids were named pET28-Tras and pET28-OKT3, respectively (Figure S2).

The coding sequence for Erv1p and DsbC without a signal sequence, which was separated by the T7-promoter sequence, was cloned into pET21-d(+), allowing for the cytoplasmic expression of both Erv1p and DsbC proteins. The resultant plasmid was named pET21-Erv1p-DsbC (Figure S3a,b).

The coding sequence for HER2 domain IV was cloned into pGEX-4T3, and the resultant plasmid was named pGEX-HER2.

The protein tethered between human CD3ε and CD3γ chains by a flexible peptide linker (the construct was denoted as hCD3εγ) was used as a CD3 construct.[38] The coding sequence for hCD3εγ was cloned into a pColdMK vector.[39] To increase the solubility during expression, a maltose-binding protein (MBP) was attached to the N-terminus of hCD3εγ. To allow for removal of MBP, an HRV3C digestion site was introduced between MBP and the hCD3εγ. A hexahistidine tag was attached to the C-terminus of hCD3εγ. The resultant vector was named pColdMK-hCD3εγ.

Expression and Purification of GST-Fusion HER2 Domain IV (GST-HER2) in E. coli. The SHuffle T7 E. coli cells (New England Biolabs) were transformed with the pGEX-HER2 plasmid. The transformed cell was selected by spreading on an LB plate containing both ampicillin (100 mg/L) and streptomycin (50 mg/L). The colony was inoculated into 50 mL of a TB medium containing ampicillin (100 mg/L) and streptomycin (50 mg/L) and cultured overnight at 30 °C. The cells were collected by centrifugation (6000 rpm, 10 min, 25 °C) and resuspended into 300 mL of a TB medium containing ampicillin (100 mg/L) and streptomycin (50 mg/L), and were stirred at 30 °C until the optical density at 600 nm reached 2.5−3.0. GST-HER2 was induced by 1 mM isopropyl β-D-1-thiogalactopyranoside (IPTG). The culture was stirred at 15 °C for more than 72 h, and then the cells were harvested by centrifugation (6000 rpm, 10 min, 4 °C), washed with 30 mL of saline, and collected again by centrifugation (6000 rpm, 20 min, 4 °C). The collected cells were suspended in 50 mM Tris−HCl (pH 8.0) with 150 mM NaCl buffer and then disrupted by sonication on ice. After centrifugation (12,000 rpm, 40 min, 4 °C), the supernatant was collected and loaded on a Glutathione Sepharose 4B column (GE Healthcare). The column was washed with a 10-bed volume (20 mL) of 50 mM Tris−HCl (pH 8.0) containing 150 mM NaCl. The GST-HER2 protein was eluted with a solution of 50 mM Tris−HCl (pH 8.0), 150 mM NaCl, and 30 mM reduced form of glutathione. The elution was collected, centrifuged (12,000 rpm, 10 min, 4 °C), and purified by gel filtration chromatography using a HiLoad 16/600 Superdex 200 pg (prep grade) column (GE Healthcare) with a running buffer of 50 mM HEPES (pH 7.4) containing 150 mM NaCl. The GST-HER2 protein was purified to a single band in the SDS-PAGE (Figure S4a).

Expression and Purification of the Tras-scFv Variants in E. coli. The SHuffle T7 *E. coli* cells were cotransformed with pET28-Tras and pET21-Erv1p-DsbC. The transformed cells were selected by spreading on an LB plate containing ampicillin (100 mg/L), kanamycin (50 mg/L), and strepto-mycin (50 mg/L). The colony was inoculated into 50 mL of a TB medium containing ampicillin (100 mg/L), kanamycin (50 mg/L), and streptomycin (50 mg/L) and cultured overnight at 30 °C. The cells were collected by centrifugation (6000 rpm, 10 min, 25 °C) and resuspended into 300 mL of a TB medium containing ampicillin (100 mg/L), kanamycin (50 mg/L), and streptomycin (50 mg/L), and stirred at 30 °C until the optical density at 600 nm reached 2.5−3.0. Tras-scFv, DsbC, and Erv1p were induced by 1 mM IPTG. The culture was stirred at 37 °C for more than 24 h, and then the cells were harvested by centrifugation (6000 rpm, 10 min, 4 °C), washed with 30 mL of saline, and collected again by centrifugation (6000 rpm, 20 min, 4 °C). The collected cells were suspended in 50 mM Tris−HCl (pH 8.0) with 150 mM NaCl buffer and then disrupted by sonication on ice. After centrifugation (12,000 rpm, 40 min, 4 °C), the supernatant was collected and loaded on a Ni-NTA agarose column. The column was washed with a 10-bed volume (20 mL) of 50 mM Tris−HCl (pH 8.0) containing both 500 mM NaCl and 20 mM imidazole. The scFv protein was eluted with a solution of 50 mM Tris−HCl (pH 8.0), 300 mM NaCl, and 250 mM imidazole. The elution was collected, centrifuged (12,000 rpm, 10 min, 4 °C), and purified by gel filtration chromatography using a HiLoad 16/600 Superdex 75 pg (prep grade) column (GE Healthcare) with a running buffer of 50 mM HEPES (pH 7.4) containing 150 mM NaCl. Tras-scFvs was purified to a single band in the SDS-PAGE analysis both under the reduced and nonreduced conditions (Figure S4b).

Expression and Purification of OKT3-scFv in E. coli. OKT3-scFv was expressed and purified by a slight modification to the method described above for Tras-scFv. After addition of IPTG, the culture was stirred at 15 °C for more than 72 h instead of at 37 °C for more than 24 h. OKT3-scFv was purified using the same protocol as for the Tras-scFv protein. All of the OKT3-scFv variants were purified to a single band in the SDS-PAGE analysis both under the reduced and nonreduced conditions (Figure S4c).

Expression and Purification of hCD3εγ in E. coli. *E. coli* strain SHuffle T7 was cotransformed with pColdMK-hCD3εγ and pET21-Erv1p-DsbC. The transformed cells were selected by spreading on an LB plate containing ampicillin (100 mg/L), kanamycin (50 mg/L), and streptomycin (50 mg/L). The colony was inoculated into 30 ml of a TB medium containing ampicillin (100 mg/L), kanamycin (50 mg/L), and strepto-mycin (50 mg/L) and cultured overnight at 30 °C. The cells were collected by centrifugation (5000 rpm, 5 min, 4 °C) and resuspended into 300 mL of a TB medium containing ampicillin (100 mg/L), kanamycin (50 mg/L), and strepto-mycin (50 mg/L), and were cultured at 30 °C until the optical density at 600 nm reached 2.5−3.0. The culture was rapidly cooled in an ice bath for 20 min, and then 1 mM IPTG was added to induce the expression of hCD3εγ, Erv1p, and DsbC, and the culture was stirred at 15 °C for more than 72 h. The cells were collected by centrifugation (6000 rpm, 15 min, 4 °C), and then washed with 20 mL of saline and resuspended in 50 mM Tris−HCl (pH 8.0) with 150 mM NaCl buffer and disrupted by sonication in an ice bath. Immediately before sonication, HRV3C protease was added to cleave MBP.

After sonication, the lysate was separated by centrifugation (12,000 rpm, 15 min, 4 °C) and loaded onto Ni-NTA agarose resin. The Ni-NTA column was washed with a 10-bed volume (20 mL) of 50 mM Tris−HCl (pH 8.0) containing both 500 mM NaCl and 20 mM imidazole, and then human CD3 was eluted by 50 mM Tris−HCl (pH 8.0), 300 mM NaCl, and 250 mM imidazole.

To completely remove MBP and the undigested product, the Ni-NTA eluent was passed through the gelatinized corn starch[39] and applied to gel filtration column chromatography using a HiLoad 16/60 Superdex 200 column (GE Healthcare) with a buffer solution containing 50 mM phosphate (pH 7.0) and 150 mM $(NH_4)_2SO_4$. The hCD3εγ protein was further purified by passing through a Butyl-S Sepharose 6 Fast Flow column (Cytiva). hCD3εγ was purified to a single band in the SDS-PAGE analysis both under the reduced and nonreduced conditions (Figure S4d).

Differential Scanning Fluorometry. Differential scan-ning fluorometry (DSF) measurement was performed as described previously.[9,10,40] All scans were obtained at a protein concentration of 3 μM in 25 mM 4-(2-hydroxyethyl)-1-piperazineethane sulfonic acid (HEPES) buffer (pH 7.4), 100 mM acetate buffer (pH 5.0), 225 mM NaCl, and SYPRO-Orange (diluted 1:1000; Sigma-Aldrich).

Surface Plasmon Resonance. Surface plasmon resonance (SPR) measurement was carried out according to a method described previously.[2,9,18,40] All SPR measurements were performed at 25 °C by using a Biacore T200 system (Cytiva). Samples were prepared with HBS-EP (10 mM HEPES pH 7.4, 150 mM NaCl, 3 mM EDTA, and 0.005% Tween 20) buffer, and GST-HER2 was immobilized on a CM5 sensor chip (Cytiva) by using a GST capture kit (Cytiva) at a flow rate of 10 μL/min. A series of various concentrations of the scFv solutions were injected into the antigen-immobilized sensor chip under a continuous flow rate of 50 μL/min.

Isothermal Titration Calorimetry. Isothermal titration calorimetry (ITC) measurement was carried out according to a method described previously.[40] Briefly, the ITC measurement between OKT3-scFv andhCD3εγ was measured with a MicroCal iTC200 (Malvern). All of the samples for ITC measurements were dialyzed against a buffer solution containing 50 mM phosphate (pH 7.0), 150 mM $(NH_4)_2SO_4$, and 5 mM EDTA. After dialysis, hCD3εγ was concentrated to 10 μM, and the cyclic scFvs were concentrated to 100 μM. Before ITC measurement, the samples were separated by centrifugation (12,000 rpm, 10 min, 4 °C), and hCD3εγ was titrated with the OKT3-scFv variants. All of the ITC data were analyzed using MicroCal Origin software (TA Instruments) with a One Set Sites Fitting Model.

RESULTS AND DISCUSSION

Strategy for the Design of Mutants. In this study, trastuzumab was used as a model antibody. Trastuzumab is a monoclonal antibody that recognizes HER2, one of the receptor tyrosine kinases of the epidermal growth factor receptor (EGFR) family.[25,26]

For the first step, an MD simulation was performed for WT Tras-scFv at 300 K to search for the weak spot, a flexible region located outside the CDR regions. In the second step, we searched for mutations that suppress flexibility by introducing new interactions around the weak spots. The CDRs are involved in antigen binding, so we excluded them as candidates for mutations. The regions located around the interface
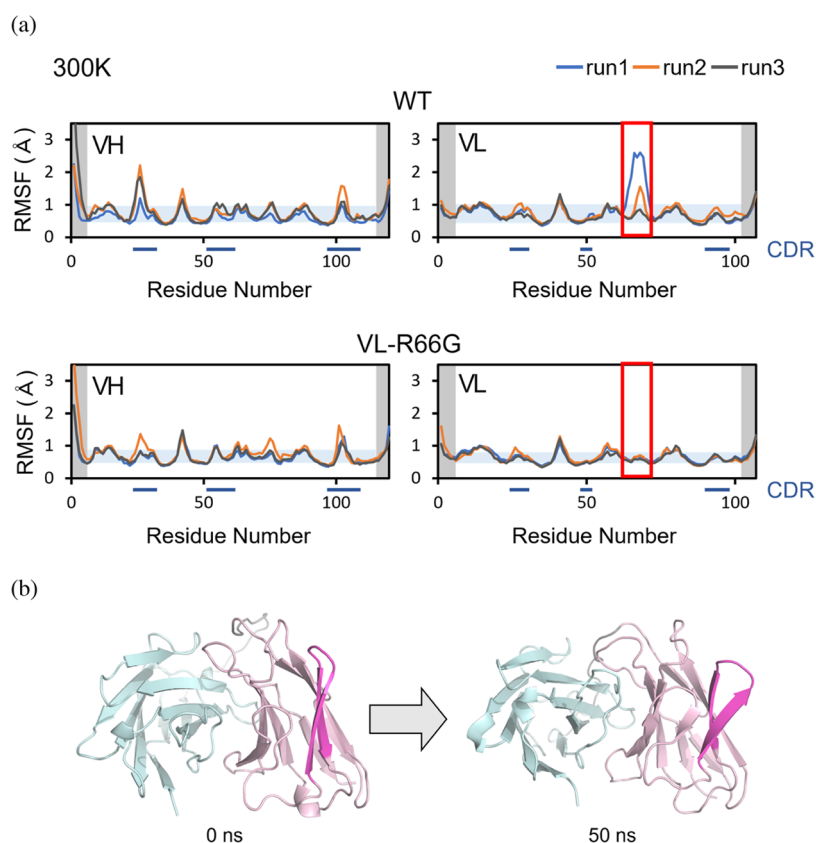
Figure 1. Search for weak spots in wild-type Tras-scFv. (a) RMSF plot of the wild-type Tras-scFv, VH region, and VL region (upper panel) and the VL-R66G mutant, VH region, and VL region (lower panel). Weak spots are enclosed in the red rectangle. The regions whose RMSF values exceeded the average values plus the standard deviations of the RMSF were defined as the regions with higher flexibility. We defined weak spots by omitting the CDRs from the region with higher flexibility. The average values plus the standard deviations of the RMSF are shown in the blue rectangle. (b) Structural change of the weak spot region (magenta). The weak spots, located around the F- and G-strand in the VL domain, were separated from the main body of the VL domain in one of the 50 ns MD simulations.

between the VH and VL domains were also omitted from the candidates for weak spots since the 50 ns MD simulation was too short for evaluating the effect of mutation around the domain interface because the open−close dynamics of the VH−VL interface is a much slower motion with longer than millisecond time scale.[9,18] The structure of the mutant, which was designed to reduce flexibility around the weak spot, was modeled by using UCSF Chimera, and the effect of the mutation was evaluated by using MD data at 300 K.

Identification of the Weak Spot Based on the MD Simulations. To search for the weak spot of Tras-scFv, three independent MD simulations were performed at 300 K for 50 ns, and the RMSF was computed (Figure 1a). The higher RMSF values indicate higher flexibility. In the first step, the average value of the RMSF was calculated with the exclusion of the respective five residues of the N- and C-termini of both the VH and VL domains. The regions whose RMSF values exceeded the average values plus the standard deviations of the RMSF were defined as the regions with higher flexibility. We defined the weak spot by omitting the CDRs from the region with higher flexibility.

As a result, the RMSF values around residues 60−70 in the VL domain were high, indicating high flexibility. In one of the MD trajectories, this region was removed from the main body of the VL domain (Figure 1b). Based on the trastuzumab Fab-HER2 complex structure, this region was not located at the antigen-binding region, and we therefore selected this region as

the weak spot to be rigidified by introduction of mutation. Despite the finding of high RMSF values around residues 40−45, this region was omitted from the candidates for weak spots since it was located around the interface between the VH and VL domains. The crystallographic B-factor is generally accepted as an index for searching for the flexible region of proteins. We found that the B-factor value was not high in the weak spot identified by the MD-based method (Figure S5) due to reduced mobility by the crystallographic packing interactions around the weak spot.[25] These results demonstrate that the RMSF analysis based on MD simulation is a powerful tool for searching for the weak spots of proteins.

Design and MD-Based Evaluation of the Thermostable Tras-scFv Mutants. To suppress flexibility around the weak spot, we mutated to introduce a new hydrogen bond. Comparison with other antibodies suggested that two hydrogen bonds, one between VL-V29 (N atom) and VL-G68 (O atom) and the other between VL-N30 (O atom) and VL-G68 (N atom) (Figure 2a), were conserved. The formation of hydrogen bonds was judged both by the atomic distance between the donor and acceptor (within 2.7−3.5 Å) and by the bond angle between the donor, the hydrogen atom, and the acceptor atom (within 120−180°).[41] At the weak spot of Tras-scFv, the hydrogen bonds could not be formed due to the bulky side chain of VL-R66. Therefore, we designed four mutants, VL-R66A, VL-R66S, VL-R66T, and VL-R66G, to eliminate steric hindrance. By changing VL-R66 to A, S, T, and
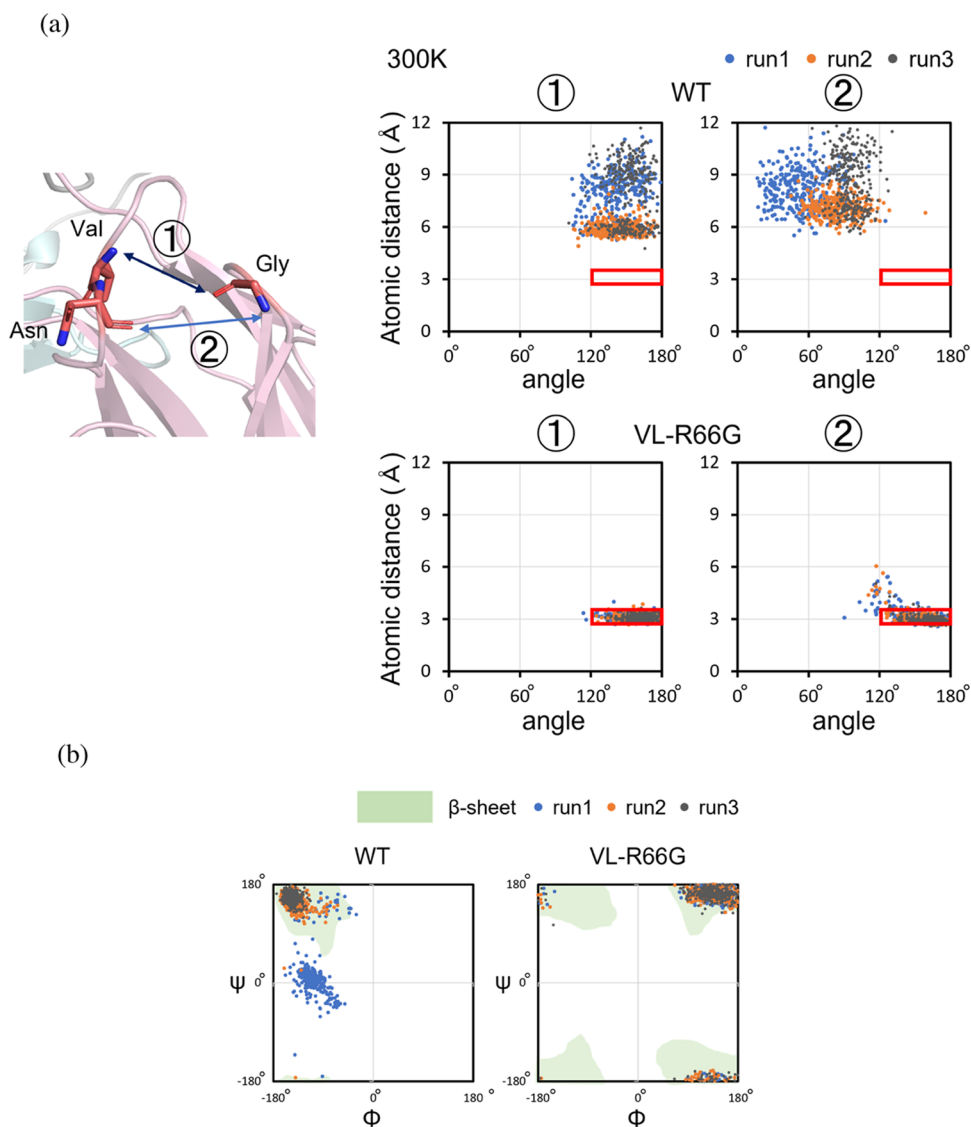
Figure 2. MD analysis of the wild-type and the VL-R66G mutant Tras-scFv. (a) Distribution of distances and angles between VL-V29 (N atom) and VL-G68 (O atom) (left panel) and between VL-N30 (O atom) and VL-G68 (N atom) (right panel) of the Tras-scFv wild-type (upper panel) and the VL-R66G mutant (lower panel). Red squares indicate regions where hydrogen bonds can be formed. (b) Ramachandran plot of VL-R66 of the wild-type Tras-scFv and VL-G66 of the VL-R-66G mutant. The β-sheet regions are shaded in green.

G, we expected that the weak spot would become closer to the main body of the VL domain and the hydrogen bonds between VL-V29 (N atom) and VL-G68 (O atom) and between VL-N30 (O atom) and VL-G68 (N atom) would be formed in the loop region of the weak spot.

The RMSF obtained from three independent MD runs for 50 ns at 300 K revealed that the flexibility at the weak spot was reduced only in VL-R66G (Figures 1a and S6a). Further, we confirmed the formation of the stable hydrogen bonds at the weak spot in VL-R66G by measuring the distances and angles between VL-V29 (N atom) and VL-G68 (O atom) and between VL-N30 (O atom) and VL-G68 (N atom) (Figures 2a and S6b).

The Ramachandran plot of the VL-66 amino acids is shown in Figure 2b. The allowed region of the β-sheet was colored green. Glycines do not possess side chains, thereby the allowed region for the β-sheet is different from other amino acids, including arginine.[42] The dihedral angle of Gly-66 of VL-R66G was in the β-sheet region of the Ramachandran plot. Based on

these observations, we selected the VL-R66G mutant for further biophysical evaluations.

Preparation and Biophysical Evaluation of the Tras-scFv VL-R66G Mutant. The melting temperature was measured by DSF, and the binding affinity to the antigen was measured by using SPR. The melting temperature of the Tras-scFv VL-R66G mutant was about 5 °C higher than that of the wild-type protein (Table 1 and Figure 3a). The binding affinity of the Tras-scFv VL-R66G mutant for the antigen was similar to that of the wild-type protein (Table 1 and Figure 3b). These results showed that we succeeded in improving

Table 1. Melting Temperature and the Binding Affinity to HER2 of Wild-Type and VL-R66G Mutant

	wild type	VL-R66G
T_m (°C)	61.8 ± 0.2	66.7 ± 0.2
ΔT_m (°C)		4.9
K_D (nM)	2.0 ± 0.4	4.8 ± 0.7

(a)

(b)
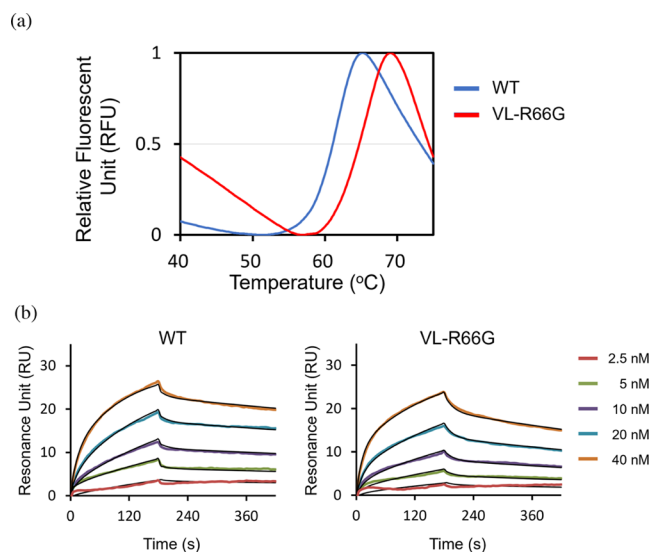
Figure 3. DSF analysis of the Tras-scFv variants and SPR analysis of the interaction between HER2 and the Tras-scFv variants. (a) DSF curve of the wild-type Tras-scFv (blue) and the VL-R66G mutant (red). (b) SPR curves of the association and dissociation of wild-type Tras-scFv to GST-HER2 immobilized on the SPR sensor chip (left panel) and the VL-R66G mutant (right panel).

thermostability without compromising the binding affinity for the antigen.

Design and Biophysical Evaluation of Cavity-Filling Mutants. To further improve the thermostability of the Tras-scFv VL-R66G mutant, we focused on VL-V33. Comparison with the other antibodies suggested that the VL-33 residue was highly occupied by either of two bulky amino acids, Ile or Leu. Hence, two mutants, VL-V33L/R66G and VL-V33I/R66G, were prepared and their thermal stability was evaluated by DSF. This analysis revealed that the melting temperature of both mutants was lower than that of VL-R66G (Table 2 and

Table 2. Melting Temperature and the Binding Affinity to HER2 of VL-R66G, VL-V33L/R66G, and VL-V33I/R66G Mutants

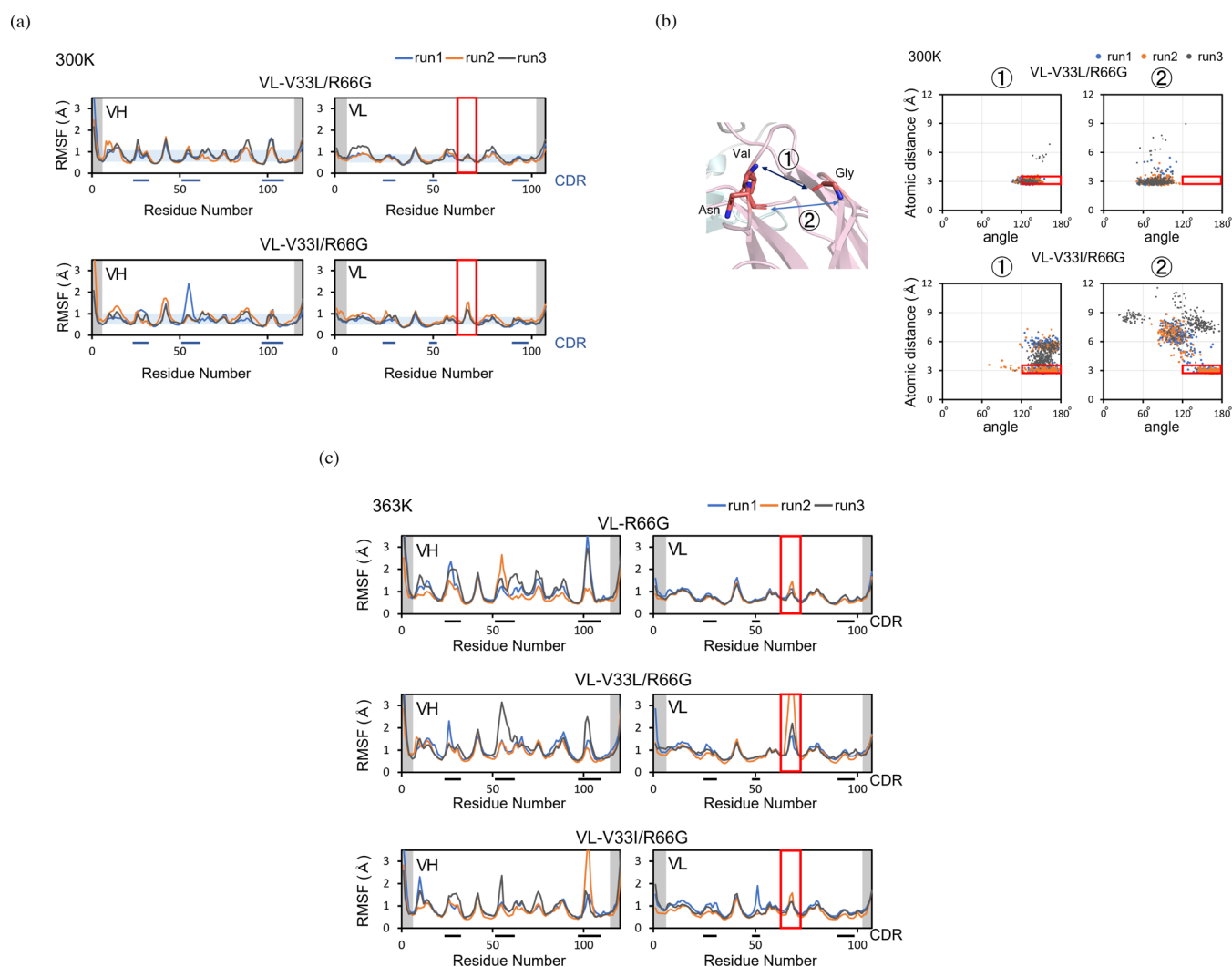|	VL-R66G	VL-V33L/R66G	VL-V33I/R66G
T_m (°C)	66.7 ± 0.2	63.8 ± 0.1	64.8 ± 0.1
ΔT_m (°C)		−2.9	−1.9
K_D (nM)	4.8 ± 0.7	4.9 ± 0.7	5.2 ± 0.4

Figure S7a), while the antigen-binding affinities were comparable (Table 2 and Figure S7b). To clarify the reason for the lower thermostabilities of VL-V33L/R66G and VL-V33I/R66G compared to Tras-scFv VL-R66G, we performed an MD simulation. The RMSF analysis revealed that VL-V33I/R66G had higher flexibility at the weak spot than the other mutants (Figure 4a). Moreover, in the Tras-scFv VL-V33I/R66G mutant, the ratio of the formation of a hydrogen bond between VL-V29 (N atom) and VL-G68 (O atom) to the formation of a hydrogen bond between VL-N30 (O atom) and VL-G68 (N atom) was lower than that in the Tras-scFv VL-R66G mutant (Figure 4b). These results were considered to explain the lower thermostability of VL-V33I/R66G compared to the Tras-scFv VL-R66G mutant. On the other hand, the RMSF analysis revealed that the VL-V33L/R66G mutant exhibited similar flexibility around the weak spot region of VL-

R66G. However, the hydrogen-bond angle between VL-V29 (N atom) and VL-G68 (O atom) was not small enough to form strong hydrogen bonds. It was also found that the angle between VL-N30 (O atom) and VL-G68 (N atom) was too small to form hydrogen bonds. These results suggest that the hydrogen bonds at the weak spot of the VL-R66G were more stable than VL-V33L/R66G. For further elucidation of the thermostability of VL-V33L/R66G, MD simulation at a higher temperature (363 K) was performed since the previous MD study of mesophilic, thermophilic, and hyperthermophilic SAICAR synthases revealed that the root-mean-square deviation (RMSD) and the RMSF values were increased and the time-averaged numbers of hydrogen bonds and salt bridges were decreased by increasing the MD temperature from 300 to 363 K in the mesophilic enzymes but not in the hyper-thermophilic enzymes,[43] and the MD data at elevated temperature were assumed to allow for the evaluation of thermostability. The RMSF at the weak spot was the highest for VL-V33L/R66G among the mutants (Figure 4c). This suggested that the thermostability at the weak spots of VL-V33L/R66G was lower among the mutants. Although further study will be required, MD simulation at a higher temperature (363 K) was useful for evaluating the stability of the weak hydrogen bonds.

■ CONCLUSIONS

In the present paper, we successfully designed thermostable mutants by evaluating the stability at the weak spots by using MD simulation. As a result, we obtained a Tras-scFv VL-R66G mutant, in which the melting temperature was increased by about 5 °C without compromising binding affinity. In a previous study, stable frameworks were successfully applied to increase the thermostability of various antibody drugs, while such a strategy was not effective for trastuzumab.[44] In our MD-based strategy, the thermal stability of Tras-scFv was successfully improved by about 5 °C. Our MD-based strategy was thus shown to be useful for obtaining thermostabilized scFv proteins. The present method was also applied for other scFv variants derived from muromonab-CD3 (OKT3), which recognizes human CD3,[38] and succeeded in obtaining the VL-H60R mutant. The VL-H60R mutant forms a stable salt bridge between VL-60R and VL-80D as compared to that of WT between VL-60H and VL-80D. The thermostability of the VL-H60R mutant was increased by about 5 °C without disrupting the antigen-binding affinity (Figure S8b and Table S2). In the case of OKT3-scFv, the weak spot could not be identified from the MD data at 300 K. Increasing the MD temperature to 333 K allowed for identification of the weak spot of the OKT3-scFv (Figure S8a). Optimization of the MD temperature was assumed to be required for each antibody. The weak spots of OKT3-scFv were located at different regions as compared to Tras-scFv. We also searched for the weak spots of another scFv derived from ipilimumab (Yervoy) and found that the weak spot was located at the same region as in Tras-scFv (Figure S9).[45] It could be assumed that the weak spot was located at a different region in each scFv protein, and we, therefore, performed a separate search for the weak spot in each antibody protein.

We next examined potential reasons for the decreased thermostability of VL-V33L/R66G and VL-V33I/R66G compared to VL-R66G by MD simulation. Simple RMSF analysis failed to predict the difference in thermal stability among Tras-scFv VL-R66G, VL-V33L/R66G, and VL-V33I/

Figure 4. MD analysis of Tras-scFv VL- R66G, VL-V33L/R66G, and VL-V33I/R66G mutants. (a) RMSF analysis of Tras-scFv VL-V33L/R66G and VL-V33I/R66G mutants. The regions whose RMSF values exceeded the average values plus the standard deviations of the RMSF were defined as the regions with higher flexibility. We defined weak spots by omitting the CDRs from the regions with higher flexibility. The average values plus the standard deviations of the RMSF are shown in the blue rectangle. (b) Distribution of distances and angles between VL-V29 (N atom) and VL-G68 (O atom) (left panel) and between VL-N30 (O atom) and VL-G68 (N atom) (right panel) of Tras-scFv VL-V33L/R66G (upper panel) and VL-V33I/R66G mutants (lower panel). Red squares indicate regions where hydrogen bonds can be formed. (c) RMSF analysis of Tras-scFv VL-R66G, VL-V33L/R66G, and VL-V33I/R66G mutants based on the MD simulations at 363 K.

R66G mutants, and thus careful evaluation of the hydrogen-bond network around the weak spot was required to explain the reason for the decrease in the thermostability of VL-V33L/R66G and VL-V33I/R66G compared to VL-R66G. These results suggested that large differences in thermostability of about 5 °C can be evaluated by RMSF at 300 K, but small differences of 2 or 3 °C require more attention.

In this study, we performed an MD simulation on the supercomputer system at Kyushu University, which is called ITO. The system consists of 2 CPUs (Intel Xeon Gold 6140, 18 cores/CPU) and 4 GPUs (NVIDIA Tesla P100, 3584 CUDA cores/GPU) per node, and we used 1 node for a single MD run. Since we used a total of 3 nodes, all of the simulations were completed within 6 h per mutant, which was a relatively short period that expended few computational resources. We identified the weak spot and evaluated the mutations by using short MD runs (50 ns, 3 runs). The number of MD runs in which at least one of the 60−70 residues of Tras-scFv exceeded the weak spot criterion was 13 of 20 MD runs versus only 4 of

20 for the Tras-scFv VL-R66G mutant (Figure S10). These results suggest that the conformational sampling was sufficient for identification and evaluation of the mutants in this study. In case the weak spot could not be identified by 50 ns MD at 300 K, as in OKT3, an MD simulation at elevated temperature would be useful. The extended-ensemble methods, e.g., accelerated MD (aMD),[46] replica exchange MD,[47] metadynamics,[48] umbrella sampling,[49] and PPI-gaMD,[50] are also available, although these require more computational resources. In the present study, the regions located around the VH−VL domain interface were omitted from the candidates for the weak spot. Although further study will be required, the application of extended-ensemble methods would be helpful for elucidation of the open−closed dynamics of the VH−VL assembly mediated by the weak VH−VL interactions, which might enable the design of a stabilization mutant located around the VH−VL interface.

Antigen-binding affinity and specificity were not evaluated by the MD simulation in this study. Although additional

investigations will be required, the MD simulation in the antigen-bound state would contribute to the evaluation of the binding affinity and specificity of the mutant. Fortunately, the mutation did not appear to have any effect on the flexibility of the CDR regions directly involved in antigen recognition in the present study (Figure 1a). This matter requires further study because, in the event that the CDR residues that are directly involved in antigen recognition were to be rigidified by mutation, the association rate constant might be reduced. Finally, the present strategy required a small number of computational resources, and it can thus be expected to make a practical contribution to the industrial application of antibodies.

■ ASSOCIATED CONTENT

Data Availability Statement

The missing atoms were constructed by using MODELLER software. The MD simulations were carried out and analyzed using the MD simulation package Gromacs 2018. The protein structures were drawn by PyMOL 2.5. The scripts and data sets are available from the following URL (https://github.com/YoshihiroKobashigawa/Okakyo_MD_data).

Ⓢ Supporting Information

The Supporting Information is available free of charge at https://pubs.acs.org/doi/10.1021/acsomega.3c01948.

> Additional experimental details (the experimental procedures, sequences, vector information, and SDS-PAGE of the proteins used in this study), biophysical data (DSF and SPR), and MD data (PDF)

■ AUTHOR INFORMATION

Corresponding Author

Hiroshi Morioka − *Department of Analytical and Biophysical Chemistry, Graduate School of Pharmaceutical Sciences, Kumamoto University, Kumamoto 862-0973, Japan;* ⓞ orcid.org/0000-0001-6931-8242; Email: morioka@gpo.kumamoto-u.ac.jp

Authors

Kyo Okazaki − *Department of Analytical and Biophysical Chemistry, Graduate School of Pharmaceutical Sciences, Kumamoto University, Kumamoto 862-0973, Japan*

Yoshihiro Kobashigawa − *Department of Analytical and Biophysical Chemistry, Graduate School of Pharmaceutical Sciences, Kumamoto University, Kumamoto 862-0973, Japan*

Hikari Morita − *Department of Analytical and Biophysical Chemistry, Graduate School of Pharmaceutical Sciences, Kumamoto University, Kumamoto 862-0973, Japan*

Soichiro Yamauchi − *Department of Analytical and Biophysical Chemistry, Graduate School of Pharmaceutical Sciences, Kumamoto University, Kumamoto 862-0973, Japan*

Natsuki Fukuda − *Department of Analytical and Biophysical Chemistry, Graduate School of Pharmaceutical Sciences, Kumamoto University, Kumamoto 862-0973, Japan*

Chenjiang Liu − *Department of Analytical and Biophysical Chemistry, Graduate School of Pharmaceutical Sciences, Kumamoto University, Kumamoto 862-0973, Japan*

Yuya Toyota − *Department of Analytical and Biophysical Chemistry, Graduate School of Pharmaceutical Sciences, Kumamoto University, Kumamoto 862-0973, Japan*

Takashi Sato − *Department of Analytical and Biophysical Chemistry, Graduate School of Pharmaceutical Sciences, Kumamoto University, Kumamoto 862-0973, Japan*

Complete contact information is available at:
https://pubs.acs.org/10.1021/acsomega.3c01948

Author Contributions

[†]K.O. and Y.K. contributed equally to the present work. K.O., Y.K., and H.M. designed the experiments. K.O., Y.K., H.M., S.Y., N.F., C.L., Y.T., and T.S. performed the experiments and analyzed the data. K.O., Y.K., and H.M. wrote the paper. All authors discussed the results.

Notes

The authors declare no competing financial interest.

■ ACKNOWLEDGMENTS

■ NOMENCLATURE

CDR, complementarity-determining region; DSF, differential scanning fluorometry; GST, glutathione S-transferase; HEPES, 4-(2-hydroxyethyl)-1-piperazineethane-sulfonic acid; HRV3C, human rhinovirus 3C; IPTG, isopropyl β-D-1-thiogalactopyranoside; ITC, isothermal titration calorimeter; KD, dissociation constant; MD, molecular dynamics; MBP, maltose-binding protein; NTA, nitrilotriacetic acid; RFU, relative fluorescence units; RMSD, root-mean-square deviation; RMSF, root-mean-square fluctuation; RU, resonance unit; scFv, single-chain variable fragment; SPR, surface plasmon resonance; TB, terrific broth; Tm, melting temperature; Tris, tris(hydroxymethyl)aminomethane; VH, variable region of the immunoglobulin heavy chain; VL, variable region of the immunoglobulin light chain

■ REFERENCES

(1) Lu, R. M.; Hwang, Y. C.; Liu, I. J.; Lee, C. C.; Tsai, H. Z.; Li, H. J.; Wu, H. C. Development of therapeutic antibodies for the treatment of diseases. *J. Biomed. Sci.* 2020, 27, No. 1.

(2) Fukuda, N.; Suwa, Y.; Uchida, M.; Kobashigawa, Y.; Yokoyama, H.; Morioka, H. Role of the mobility of antigen binding site in high affinity antibody elucidated by surface plasmon resonance. *J. Biochem.* 2017, 161, 37−43.

(3) Huston, J. S.; Levinson, D.; Mudgett-Hunter, M.; Tai, M. S.; Novotný, J.; Margolies, M. N.; Ridge, R. J.; Bruccoleri, R. E.; Haber, E.; Crea, R. Protein engineering of antibody binding sites: Recovery of specific activity in an anti-digoxin single-chain Fv analogue produced in *Escherichia coli*. *Proc. Natl. Acad. Sci. U.S.A.* 1988, 85, 5879−5883.

(4) Jermutus, L.; Honegger, A.; Schwesinger, F.; Hanes, J.; Plückthun, A. Tailoring in vitro evolution for protein affinity or stability. *Proc. Natl. Acad. Sci. U.S.A.* 2001, 98, 75−80.

(5) Plückthun, A.; Skerra, A. Expression of functional antibody Fv and Fab fragments in *Escherichia coli*. *Methods Enzymol.* 1989, 178, 497−515.

(6) Kobayashi, H.; Morioka, H.; Tobisawa, K.; Torizawa, T.; Kato, K.; Shimada, I.; Nikaido, O.; Stewart, J. D.; Ohtsuka, E. Probing the interaction between a high-affinity single-chain Fv and a pyrimidine (6-4) pyrimidone photodimer by site-directed mutagenesis. *Biochemistry* 1999, 38, 532−539.

(7) Röthlisberger, D.; Honegger, A.; Plückthun, A. Domain interactions in the Fab fragment: a comparative evaluation of the single-chain Fv and Fab format engineered with variable domains of different stability. *J. Mol. Biol.* **2005**, *347*, 773−789.

(8) Quintero-Hernández, V.; Juárez-González, V. R.; Ortíz-León, M.; Sánchez, R.; Possani, L. D.; Becerril, B. The change of the scFv into the Fab format improves the stability and in vivo toxin neutralization capacity of recombinant antibodies. *Mol. Immunol.* **2007**, *44*, 1307−1315.

(9) Yamauchi, S.; Kobashigawa, Y.; Fukuda, N.; Teramoto, M.; Toyota, Y.; Liu, C.; Ikeguchi, Y.; Sato, T.; Sato, Y.; Kimura, H.; Masuda, T.; Ohtsuki, S.; Noi, K.; Ogura, T.; Morioka, H. Cyclization of single-chain Fv antibodies markedly suppressed their characteristic aggregation mediated by inter-chain VH-VL interactions. *Molecules* **2019**, *24*, No. 2620.

(10) Liu, C.; Kobashigawa, Y.; Yamauchi, S.; Fukuda, N.; Sato, T.; Masuda, T.; Ohtsuki, S.; Morioka, H. Convenient method of producing cyclic single-chain Fv antibodies by split-intein-mediated protein ligation and chaperone co-expression. *J. Biochem.* **2020**, *168*, 257−263.

(11) Weatherill, E. E.; Cain, K. L.; Heywood, S. P.; Compson, J. E.; Heads, J. T.; Adams, R.; Humphreys, D. P. Towards a universal disulphide stabilised single chain Fv format: importance of interchain disulphide bond location and vL−vH orientation. *Protein Eng., Des. Sel.* **2012**, *25*, 321−329.

(12) Young, N. M.; MacKenzie, C. R.; Narang, S. A.; Oomen, R. P.; Baenziger, J. E. Thermal stabilization of a single-chain Fv antibody fragment by introduction of a disulphide bond. *FEBS Lett.* **1995**, *377*, 135−139.

(13) Wörn, A.; Plückthun, A. Different equilibrium stability behavior of ScFv fragments: identification, classification, and improvement by protein engineering. *Biochemistry* **1999**, *38*, 8739−8750.

(14) Rajagopal, V.; Pastan, I.; Kreitman, R. J. A form of anti-Tac (Fv) which is both single-chain and disulfide stabilized: comparison with its single-chain and disulfide-stabilized homologs. *Protein Eng., Des. Sel.* **1997**, *10*, 1453−1459.

(15) Ewert, S.; Honegger, A.; Plückthun, A. Stability improvement of antibodies for extracellular and intracellular applications: CDR grafting to stable frameworks and structure-based framework engineering. *Methods* **2004**, *34*, 184−199.

(16) Jespers, L.; Schon, O.; Famm, K.; Winter, G. Aggregation-resistant domain antibodies selected on phage by heat denaturation. *Nat. Biotechnol.* **2004**, *22*, 1161−1165.

(17) Famm, K.; Hansen, L.; Christ, D.; Winter, G. Thermodynamically stable aggregation-resistant antibody domains through directed evolution. *J. Mol. Biol.* **2008**, *376*, 926−931.

(18) Fukuda, N.; Noi, K.; Weng, L.; Kobashigawa, Y.; Miyazaki, H.; Wakeyama, Y.; Takaki, M.; Nakahara, Y.; Tatsuno, Y.; Uchida-Kamekura, M.; Suwa, Y.; Sato, T.; Ichikawa-Tomikawa, N.; Nomizu, M.; Fujiwara, Y.; Ohsaka, F.; Saitoh, T.; Maenaka, K.; Kumeta, H.; Shinya, S.; Kojima, C.; Ogura, T.; Morioka, H. Production of single-chain Fv antibodies specific for GA-Pyridine, an advanced glycation end-product (AGE), with reduced inter-domain motion. *Molecules* **2017**, *22*, No. 1695.

(19) Graff, C. P.; Chester, K.; Begent, R.; Wittrup, K. D. Directed evolution of an anti-carcinoembryonic antigen scFv with a 4-day monovalent dissociation half-time at 37 degrees C. *Protein Eng., Des. Sel.* **2004**, *17*, 293−304.

(20) Chao, G.; Lau, W. L.; Hackel, B. J.; Sazinsky, S. L.; Lippow, S. M.; Wittrup, K. D. Isolating and engineering human antibodies using yeast surface display. *Nat. Protoc.* **2006**, *1*, 755−768.

(21) Dudgeon, K.; Rouet, R.; Kokmeijer, I.; Schofield, P.; Stolp, J.; Langley, D.; Stock, D.; Christ, D. General strategy for the generation of human antibody variable domains with increased aggregation resistance. *Proc. Natl. Acad. Sci. U.S.A.* **2012**, *109*, 10879−10884.

(22) Miller, B. R.; Demarest, S. J.; Lugovskoy, A.; Huang, F.; Wu, X.; Snyder, W. B.; Croner, L. J.; Wang, N.; Amatucci, A.; Michaelson, J. S.; Glaser, S. M. Stability engineering of scFvs for the development of bispecific and multivalent antibodies. *Protein Eng., Des. Sel.* **2010**, *23*, 549−557.

(23) Bekker, G. J.; Ma, B.; Kamiya, N. Thermal stability of single-domain antibodies estimated by molecular dynamics simulations. *Protein Sci.* **2019**, *28*, 429−438.

(24) Ikeuchi, E.; Kuroda, D.; Nakakido, M.; Murakami, A.; Tsumoto, K. Delicate balance among thermal stability, binding affinity, and conformational space explored by single-domain VHH antibodies. *Sci. Rep.* **2021**, *11*, No. 20624.

(25) Cho, H. -S.; Mason, S.; Ramyar, K. X.; Stanley, A. M.; Gabelli, S. B.; Denney, D. W., Jr.; Leahy, D. J. Structure of the extracellular region of HER2 alone and in complex with the Herceptin Fab. *Nature* **2003**, *421*, 756−760.

(26) Li, Y. M.; Pan, Y.; Wei, Y.; Cheng, X.; Zhou, B. P.; Tan, M.; Zhou, X.; Xia, W.; Hortobagyi, G. N.; Yu, D.; Hung, M. C. Upregulation of CXCR4 is essential for HER2-mediated tumor metastasis. *Cancer Cell* **2004**, *6*, 459−469.

(27) Eswar, N.; Webb, B.; Marti-Renom, M. A.; Madhusudhan, M. S.; Eramian, D.; Shen, M. Y.; Pieper, U.; Sali, A. Comparative protein structure modeling using MODELLER. *Curr. Protoc. Protein Sci.* **2007**, *50*, 2.9.1−2.9.31.

(28) Martí-Renom, M. A.; Stuart, A. C.; Fiser, A.; Sánchez, R.; Melo, F.; Sali, A. Comparative protein structure modeling of genes and genomes. *Annu. Rev. Biophys. Biomol. Struct.* **2000**, *29*, 291−325.

(29) Šali, A.; Blundell, T. L. Comparative protein modelling by satisfaction of spatial restraints. *J. Mol. Biol.* **1993**, *234*, 779−815.

(30) Pettersen, E. F.; Goddard, T. D.; Huang, C. C.; Couch, G. S.; Greenblatt, D. M.; Meng, E. C.; Ferrin, T. E. UCSF Chimera - A visualization system for exploratory research and analysis. *J. Comput. Chem.* **2004**, *25*, 1605−1612.

(31) Abraham, M. J.; Murtola, T.; Schulz, R.; Páll, S.; Smith, J. C.; Hess, B.; Lindahl, E. GROMACS: High performance molecular simulations through multi-level parallelism from laptops to super-computers. *SoftwareX* **2015**, *1−2*, 19−25.

(32) Huang, J.; Rauscher, S.; Nawrocki, G.; Ran, T.; Feig, M.; de Groot, M. L.; Grubmüller, H.; MacKerell, A. D., Jr. CHARMM36m: an improved force field for folded and intrinsically disordered proteins. *Nat. Methods* **2017**, *14*, 71−73.

(33) MacKerell, A. D., Jr.; Feig, M.; Brooks, C. L., III Improved treatment of the protein backbone in empirical force fields. *J. Am. Chem. Soc.* **2004**, *126*, 698−699.

(34) Darden, T.; York, D.; Pedersen, L. Particle mesh Ewald: An N·log(N) method for Ewald sums in large systems. *J. Chem. Phys.* **1993**, *98*, 10089−10092.

(35) Hess, B.; Bekker, H.; Berendsen, H. J. C.; Fraaije, J. G. E. M. LINCS: A Linear Constraint Solver for molecular simulations. *J. Comput. Chem.* **1997**, *18*, 1463−1472.

(36) Humphrey, W.; Dalke, A.; Schulten, K. VMD: Visual molecular dynamics. *J. Mol. Graphics* **1996**, *14*, 33−38.

(37) Trigoso, Y. D.; Evans, R. C.; Karsten, W. E.; Chooback, L. Cloning, Expression, and Purification of Histidine-Tagged *Escherichia coli* Dihydrodipicolinate Reductase. *PLoS One* **2016**, *11*, No. e0146525.

(38) Kjer-Nielsen, L.; Dunstone, M. A.; Kostenko, L.; Ely, L. K.; Beddoe, T.; Mifsud, N. A.; Purcell, A. W.; Brooks, A. G.; McCluskey, J.; Rossjohn, J. Crystal structure of the human T cell receptor CD3εγ heterodimer complexed to the therapeutic mAb OKT3. *Proc. Natl. Acad. Sci. U S A.* **2004**, *101*, 7675−7680.

(39) Kobashigawa, Y.; Namikawa, M.; Sekiguchi, M.; Inada, Y.; Yamauchi, S.; Kimoto, Y.; Okazaki, K.; Toyota, Y.; Sato, T.; Morioka, H. Expression, purification and characterization of CAR/NCOA-1 tethered protein in *E. coli* using maltose-binding protein fusion tag and gelatinized corn starch. *Biol. Pharm. Bull.* **2021**, *44*, 125−130.

(40) Kobashigawa, Y.; Ohara, T.; Morita, K.; Toyota, Y.; Nakamura, T.; Kotani, S.; Arimori, T.; Yamauchi, S.; Liu, C.; Kitazaki, M.; Wakeyama-Miyazaki, Y.; Suwa, Y.; Uchida-Kamekura, M.; Fukuda, N.; Sato, T.; Nakajima, M.; Takagi, J.; Yamagata, Y.; Morioka, H. Molecular recognition of a single-chain Fv antibody specific for GA-pyridine, an advanced glycation end-product (AGE), elucidated using

biophysical techniques and synthetic antigen analogues. *J. Biochem.* **2021**, *170*, 379−387.

(41) Yoshida, K.; Kuroda, D.; Kiyoshi, M.; Nakakido, M.; Nagatoishi, S.; Soga, S.; Shirai, H.; Tsumoto, K. Exploring designability of electrostatic complementarity at an antigen-antibody interface directed by mutagenesis, biophysical analysis, and molecular dynamics simulations. *Sci. Rep.* **2019**, *9*, No. 4482.

(42) Lovell, S. C.; Davis, I. W.; Arendall, W. B., III; de Bakker, P. I. W.; Word, J. M.; Prisant, M. G.; Richardson, J. S.; Richardson, D. C. Structure Validation by Cα Geometry: φ,ψ and Cβ Deviation. *Proteins* **2003**, *50*, 437−450.

(43) Manjunath, K.; Sekar, K. Molecular dynamics perspective on the protein thermal stability: A case study using SAICAR synthetase. *J. Chem. Inf. Model.* **2013**, *53*, 2448−2461.

(44) McConnell, A. D.; Zhang, X.; Macomber, J. L.; Chau, B.; Sheffer, J. C.; Rahmanian, S.; Hare, E.; Spasojevic, V.; Horlick, R. A.; King, D. J.; Bowers, P. M. A general approach to antibody thermostabilization. *MAbs* **2014**, *6*, 1274−1282.

(45) He, M.; Chai, Y.; Qi, J.; Zhang, C. W. H.; Tong, Z.; Shi, Y.; Yan, J.; Tan, S.; Gao, G. F. Remarkably similar CTLA-4 binding properties of therapeutic ipilimumab and tremelimumab antibodies. *Oncotarget* **2017**, *8*, 67129−67139.

(46) Pierce, L. C. T.; Salomon-Ferrer, R.; de Oliveira, C. A. F.; McCammon, J. A.; Walker, R. C. Routine access to millisecond time scale events with accelerated molecular dynamics. *J. Chem. Theory Comput.* **2012**, *8*, 2997−3002.

(47) Sugita, Y.; Yuko, O. Replica-exchange molecular dynamics method for protein folding. *Chem. Phys. Lett.* **1999**, *314*, 141−151.

(48) Laio, A.; Parrinello, M. Escaping free-energy minima. *Proc. Natl. Acad. Sci. U.S.A.* **2002**, *99*, 12562−12566.

(49) Kästner, J. Umbrella sampling. *Wiley Interdiscip. Rev.: Comput. Mol. Sci.* **2011**, *1*, 932−942.

(50) Wang, J.; Miao, Y. Protein-Protein Interaction-Gaussian Accelerated Molecular Dynamics (PPI-GaMD): Characterization of Protein Binding Thermodynamics and Kinetics. *J. Chem. Theory Comput.* **2022**, *18*, 1275−1285.